

PERFORMANCE AND UNCERTAINTY EVALUATION OF OPTICAL COORDINATE METROLOGY FOR HYBRID MANUFACTURING

Jake Dvorak¹, Ross Zamoski¹, and Tony Schmitz^{1,2}

¹Department of Mechanical, Aerospace, and Biomedical Engineering
University of Tennessee, Knoxville
Knoxville, TN 37996, USA

²Manufacturing Demonstration Facility
Oak Ridge National Laboratory
Oak Ridge, TN, 37830, USA

INTRODUCTION

Additive manufacturing (AM) produces complex, near net shape geometries, but AM preforms must generally be machined to meet the required dimensional accuracy and surface finish for production-quality components. A persistent challenge, especially for hybrid manufacturing using separate AM and milling machines, is identifying the part location within the machine tool's work volume using the same coordinate systems as the computer numerical control (CNC) machining toolpaths to produce the designer's intended geometry. This research defines and assesses a framework for measurement, coordinate system identification, and toolpath generation for sequential hybrid manufacturing using optical coordinate metrology; see procedure in Fig. 1 [1].

Performance of four optical coordinate metrology systems are evaluated based on relevant VDI/VDE standards [2]. A single metric, the uncertainty in a sphere's center position, is selected as the basis for the evaluation. This metric is used in a Monte Carlo simulation to estimate the origin and orientation variation of coordinate systems defined using three fiducial spheres in hybrid manufacturing. This simulation estimates the additional AM material (overbuild) needed to ensure the final geometry is contained within the preform using the selected CNC toolpath. The overbuild is defined in the form of a bounding box that incorporates the scanner uncertainty in the hybrid process. This research advances the ability to apply optical coordinate metrology for defining coordinate systems and stock models in hybrid manufacturing.

PERFORMANCE AND UNCERTAINTY EVALUATION

Evaluating the performance of optical coordinate metrology systems is challenging because many

factors affect the measurement results, including but not limited to: temperature, vibration, point cloud processing, object reflectivity, scanner calibration, and operator method [3]. ISO Standard 10360-13, Geometrical product specifications (GPS) — Acceptance and reverification tests for coordinate measuring systems (CMS) and VDI/VDE 2634 Part 2 and 3

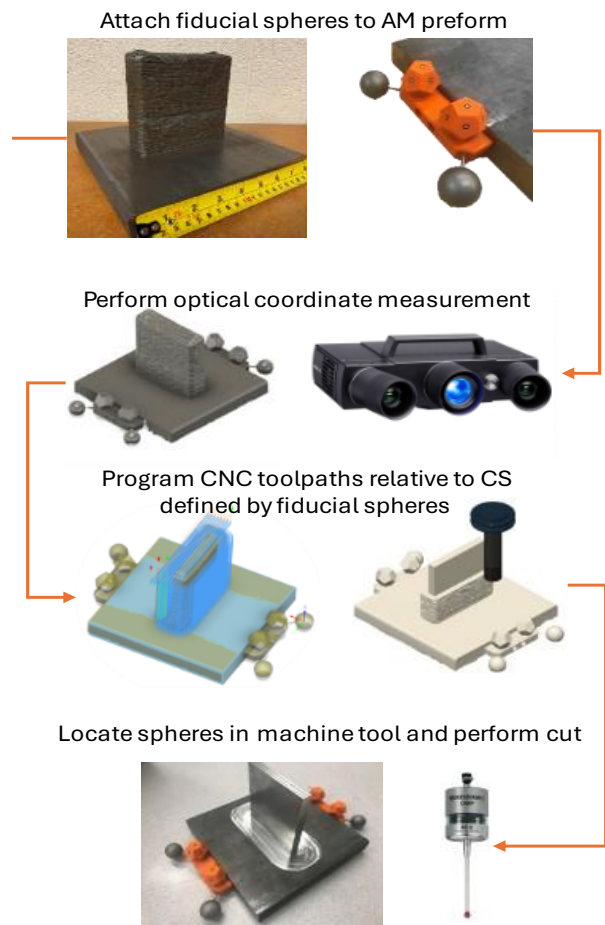


FIGURE 1. Process flow for sequential hybrid manufacturing.

define four quality parameters to quantify optical coordinate measurement performance; see Fig. 2. This work reports these parameters for four optical coordinate metrology systems: a ZEISS ATOS Q, a ZEISS Core 200, an Artec Spider, and an iPhone 15 Pro Max. The quality parameters are evaluated using a ball bar sized to the scanner's measurement volume.

The first quality parameter, probing error form, PF , is the range of radial distances of measured points to a calculated fitted sphere center determined by the least-squares method; see Fig. 2, bottom right. Generally, probing error contains two influences: errors within singular measurements inside the measurement volume and errors due to transformations of single measurements.

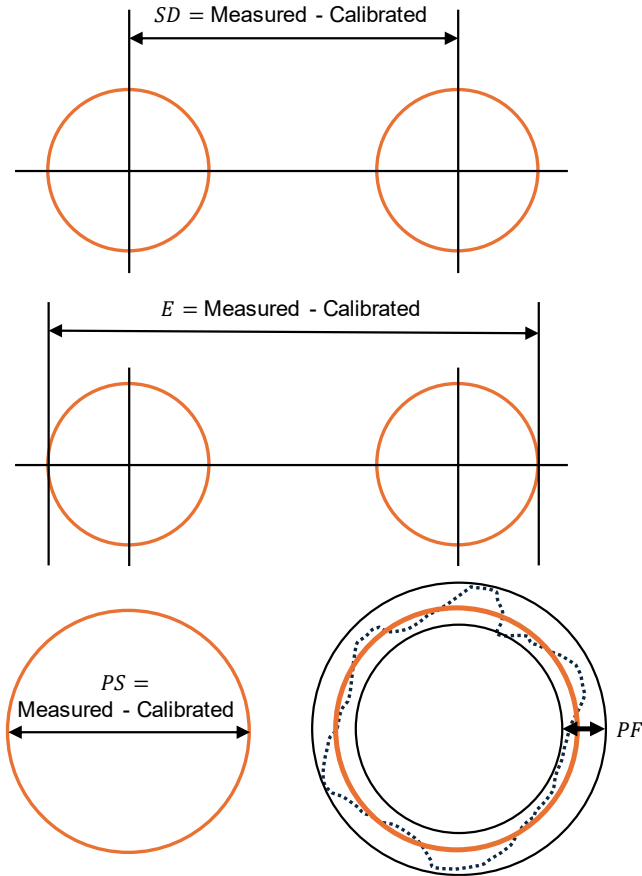


FIGURE 2. Metrics for optical coordinate measurement system performance evaluation, including sphere spacing error (top), length measurement error (center), probing error size (bottom left), and probing error form (bottom right).

Probing error size, PS , is the difference between the measured diameter of a fitted sphere determined by the least-squares method and the calibrated diameter of the sphere; see Fig. 2, bottom left. It is formally defined as the difference between the fitted diameter, D_a , and the calibrated diameter, D_t ; see Eq. 1.

$$PS = D_a - D_t \quad (1)$$

Sphere spacing error, SD , is the difference between the measured value and the calibrated value of the distance (or spacing) between the centers of two spheres; see Fig. 2, top. This describes the ability of the measuring system to perform length measurements from multiple single images and is defined in Eq. 2,

$$SD = L_{ka} - L_{kr} \quad (2)$$

where L_{ka} is the measured sphere spacing distance and L_{kr} is the calibrated sphere spacing distance.

Length measurement error, E , can be found when bidirectional probing is performed from two opposite points along the axis defined by the two fit sphere center points; see Fig. 2, center. This describes the error behavior over the entire measuring volume due to a combination of various single errors. Some examples include systematic errors, random errors, and multiple scan stitching/alignment.

Method C in VDI/VDE 2634 part 3 describes correction for the averaging effect and compensation for systematic probing errors when ball bars with only two balls are used. The length measurement error E is shown in Eq. 3.

$$E = SD + E_k \quad (3)$$

E_k is a correction defined in Eq. 4,

$$E_k = \frac{R_1 - D_{r1}}{2} + \frac{R_2 - D_{r2}}{2} \quad (4)$$

where D_{r1} and D_{r2} are the calibrated diameters of the two spheres and R_1 and R_2 are spacings of two selected points to the fit sphere centers. These two points are selected as outer edge points on the spheres with minimum spacing from the center using a straight line through the sphere center. In other words, the length measurement error accounts for identifying the closest point in

the point cloud data that provides the end-to-end probing length.

MONTE CARLO SIMULATION

A Monte Carlo simulation was prepared to evaluate variation in the origin and orientation of a coordinate system defined using the centers of three fiducial spheres. This coordinate system is used to connect the preform, desired part geometry, and machine tool; see Fig. 1. The simulation produces standard deviations of the origin's translation and rotations about the three axes by calculating the homogeneous transformation matrix (HTM) between the nominal and actual coordinate systems using the nominal and simulated sphere positions. The standard deviation of probing error form, the nominal sphere positions, and the work volume are the simulation inputs. Additionally, the simulation finds the distribution of required overbuild (or bounding box) to account for uncertainty in the coordinate system.

In each iteration of the simulation, i , the center position for each of the three fiducial spheres is randomly sampled from a normal distribution based on the sphere center uncertainty. The nominal (X,Y,Z) positions of three fiducial sphere centers are defined as $S_{1,nominal}$, $S_{2,nominal}$, and $S_{3,nominal}$. Basis vectors of the nominal coordinate system are calculated; see Fig. 3. The X direction is defined using sphere 2 and sphere 1 such that

$$X_{nominal} = \frac{S_{2,nominal} - S_{1,nominal}}{\|S_{2,nominal} - S_{1,nominal}\|} \quad (5)$$

A vector is defined from sphere 3 to sphere 1 such that

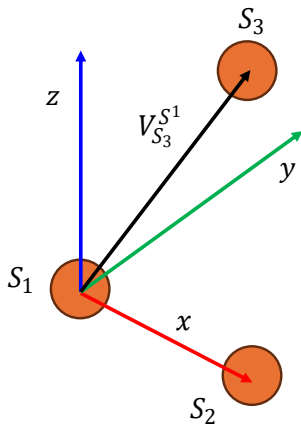


FIGURE 3. Basis vector definition for nominal coordinate system defined by three sphere centers.

$$V_{S_3, nominal}^{S_1, nominal} = \frac{S_{3, nominal} - S_{1, nominal}}{\|S_{3, nominal} - S_{1, nominal}\|} \quad (6)$$

The Z direction is defined as the cross product of X and $V_{S_3}^{S_1}$ so that

$$Z_{nominal} = \frac{X_{nominal} \times V_{S_3, nominal}^{S_1, nominal}}{\|X_{nominal} \times V_{S_3, nominal}^{S_1, nominal}\|} \quad (7)$$

The Y direction is

$$Y_{nominal} = Z_{nominal} \times X_{nominal} \quad (8)$$

The nominal rotation matrix becomes

$$R_{nominal} = [X_{nominal} \ Y_{nominal} \ Z_{nominal}] \quad (9)$$

The same procedure is repeated for $S_{1-3, simulated}$ such that

$$S_{1-3, simulated, i} = S_{1-3, nominal} + P_{1-3, simulated, i} \quad (10)$$

where $P_{1-3, simulated, i}$ are each a random number sampled from the normal distribution with mean 0 and standard deviation of $\frac{\sigma_{PF}}{2}$ where σ_{PF} is the standard deviation of the probing error form. By following the same procedure as Equations 5-9, the rotation matrix between simulated and nominal coordinate systems becomes

$$R_{simulated, i}^{nominal} = \frac{R_{simulated, i}}{R_{nominal}} \quad (11)$$

Translation from the nominal to simulated coordinate system origins, or translations error, is

$$\delta_i = S_{1, simulated, i} - R_{simulated, i}^{nominal} S_{1, nominal, i} \quad (12)$$

The Euler angles (ZYX angles) between the simulated and nominal coordinate system become the rotational errors $\varepsilon_{x, i}$, $\varepsilon_{y, i}$, and $\varepsilon_{z, i}$. With correlation neglected between standard uncertainties and a coverage factor, k , the expanded uncertainties for translation and rotation become

$$U_\delta = k \sqrt{\sigma_{\delta_x}^2 + \sigma_{\delta_y}^2 + \sigma_{\delta_z}^2} \quad (13)$$

$$U_\varepsilon = k \sqrt{\sigma_{\varepsilon_x}^2 + \sigma_{\varepsilon_y}^2 + \sigma_{\varepsilon_z}^2} \quad (14)$$

Additionally, the required overbuild to compensate for the simulated variation is found; see Fig. 4. The homogeneous transformation matrix is

$$T_i = \begin{pmatrix} R_{simulated}^{nominal} & \delta_i \\ 0 & 1 \end{pmatrix} \quad (15)$$

An overbuild value, O_b , is increased incrementally until $P_{min,nominal} \geq P_{min,simulated}$ and $P_{max,nominal} \leq P_{max,simulated}$ where

$$P_{min,simulated,i} = T_i \begin{pmatrix} P_{min,x} - O_b \\ P_{min,y} - O_b \\ P_{min,z} - O_b \\ 1 \end{pmatrix} \quad (16)$$

and

$$P_{max,simulated,i} = T_i \begin{pmatrix} P_{max,x} + O_b \\ P_{max,y} + O_b \\ P_{max,z} + O_b \\ 1 \end{pmatrix} \quad (17)$$

The result is a distribution of required overbuild quantities $O_{b,i}$ for all Monte Carlo simulation iterations.

NOMINAL PART ORIENTATION

SIMULATED PART ORIENTATION

REQUIRED OVERBUILD
IN NOMINAL CS

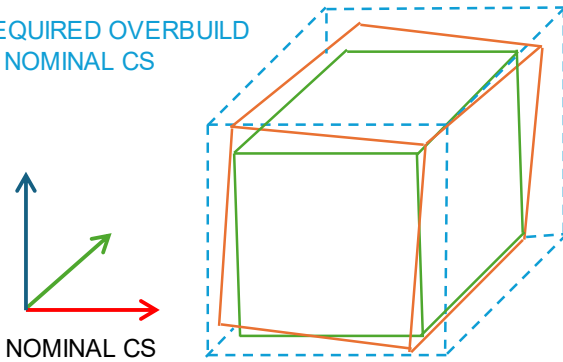


FIGURE 4. Required overbuild to compensate for measurement uncertainty.

EXPERIMENTAL SETUP

Simulation results were verified experimentally from repeated measurements of a calibrated artifact (ZEISS PSA 400) containing multiple ball bars (sphere pairs); see Fig. 5. The range of ball bar lengths enabled selection of an optimal pair of spheres for each measurement system based on its measurement volume. By using adjacent spheres to this optimal pair, a left and right coordinate system could be defined for each

measurement system; see Fig. 6. Error between the translation and rotation between the left and right coordinate systems is based on measurements with a touch probe coordinate measurement machine (CMM) and the optical coordinate measurement (OCM) system.



FIGURE 5. ZEISS PSA 400 artifact used for performance evaluation.

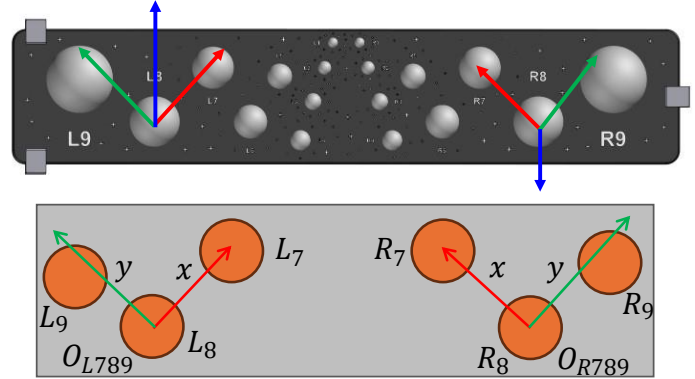


FIGURE 6. Example left and right coordinate system defined on PSA400 artifact.

RESULTS

The average quality parameters for each OCM system's optimal pair from three data sets are shown in Fig. 7. The results quantitatively show the difference in performance between the OCM systems considered in this study. Since these results are for each scanner's optimal pair, the metrics are approximately normalized to scanner volume.

The Monte Carlo simulation was completed over 5×10^5 iterations for each OCM system. Half of standard deviation of probing error form found for each OCM system was used for generating the distributions for the sphere center positions. Experimental results are plotted with simulation results in Fig. 8 with a coverage factor $k = 2$. Good agreement is observed between experimental and simulated uncertainties. Note that results are shown for the ATOS Q with both spot and matrix metering, which represent two

different auto-exposure approaches. The difference in results for these two metering settings demonstrates the importance of proper exposure to achieving accurate results, and that the influence of this setting on uncertainty can be substantial.

Figure 9 shows results for overbuild simulations for all OCM systems for a 100 mm x 100 mm x 100 mm part placed at the max distance of respective scan volume. It is seen that the ATOS Q and ATOS Core would require approximately 35 μm of overbuild to fully compensate for their uncertainties. The Spider requires approximately 150 μm of overbuild and the iPhone over 25 mm.

CONCLUSIONS

Hybrid manufacturing has been demonstrated to provide a viable option for traditional manufacturing solutions that face global supply chain challenges. While hybrid processes on a single machine tool are becoming readily available, research and discussion on how to use different machine tools sequentially is still required and is defined here as sequential hybrid manufacturing. This work represents a major step forward in validation and adoption of sequential hybrid manufacturing by means of Monte Carlo simulations and experimental validations of coordinate system translational and rotational uncertainties, and evaluation of fiducial sphere center positional uncertainties using optical coordinate metrology systems. A function to estimate required overbuild in the AM step to compensate for sphere center uncertainty due to the optical coordinate measurement system used is implemented. This work universally applies to any AM + X scenario that uses three fiducial spheres and OCM for CS definition and transfer.

ACKNOWLEDGEMENTS

The authors acknowledge support from the NSF Engineering Research Center for Hybrid Autonomous Manufacturing Moving from Evolution to Revolution (ERC-HAMMER) under Award Number EEC2133630.

REFERENCES

- [1] Dvorak, Jake, "Feasibility and uncertainty evaluation of sequential hybrid manufacturing using optical coordinate metrology." PhD diss., University of Tennessee, 2024.
- [2] "VDI/VDE 2634 Part 3: Optical 3D-measuring systems - Multiple view systems based on area scanning."

- [3] Y. Zhao, Y. Cheng, Q. Xu, Z. Luo, X. Wang, and H. Li, "Uncertainty modeling and evaluation of profile measurement by structured light scanner," *Measurement Science and Technology*, vol. 33, no. 9, p. 095018, 2022.

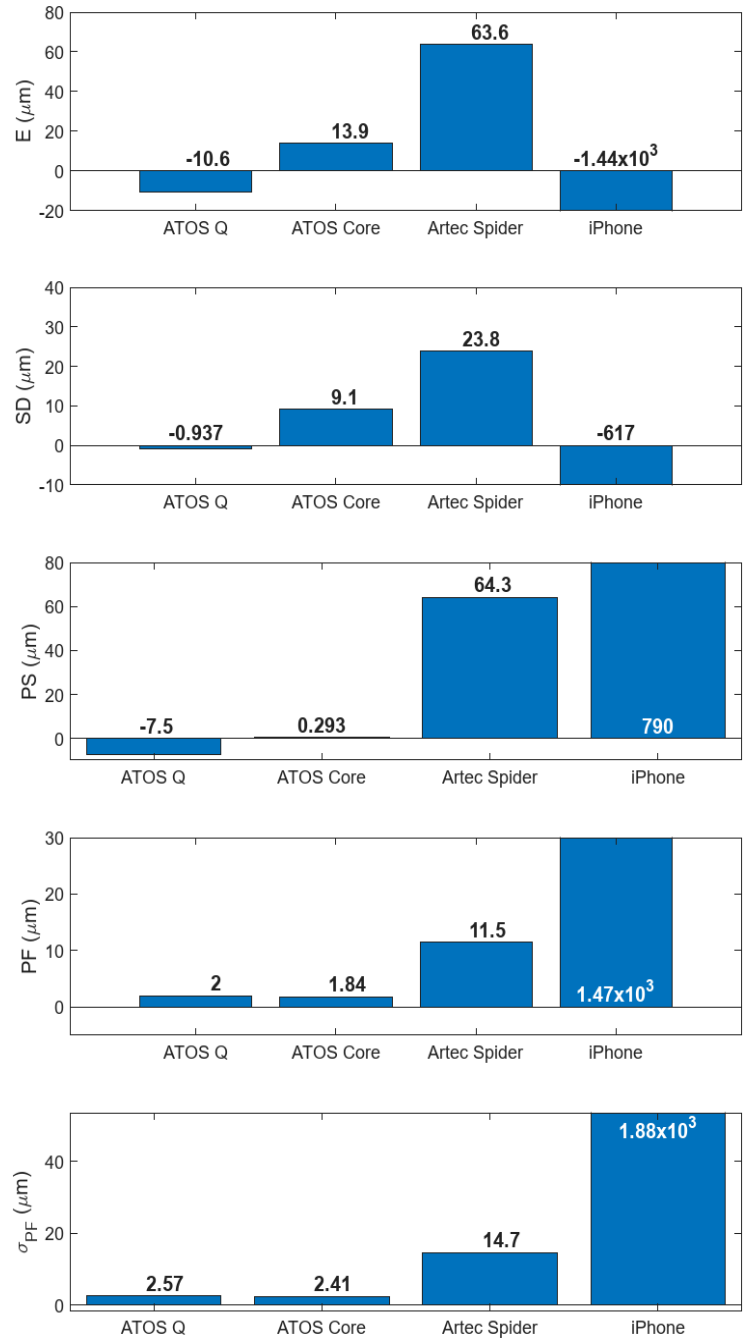


FIGURE 7. Performance evaluation results.

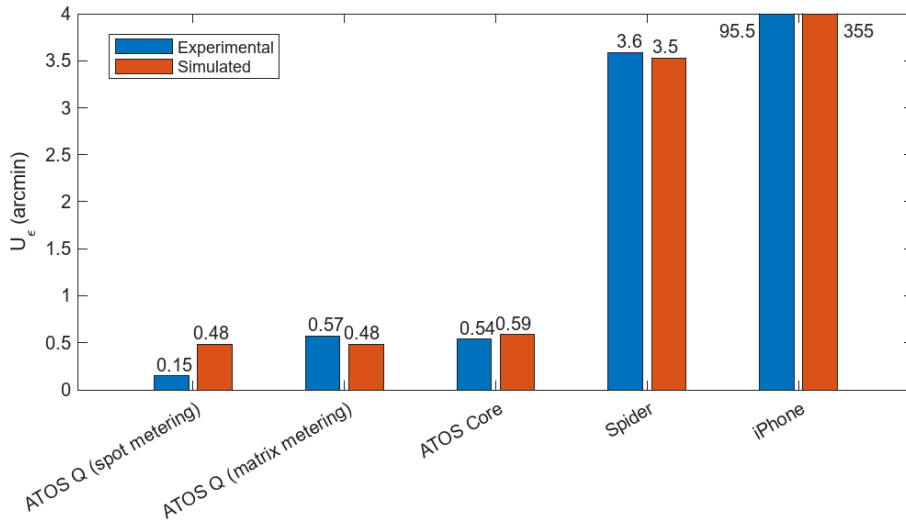
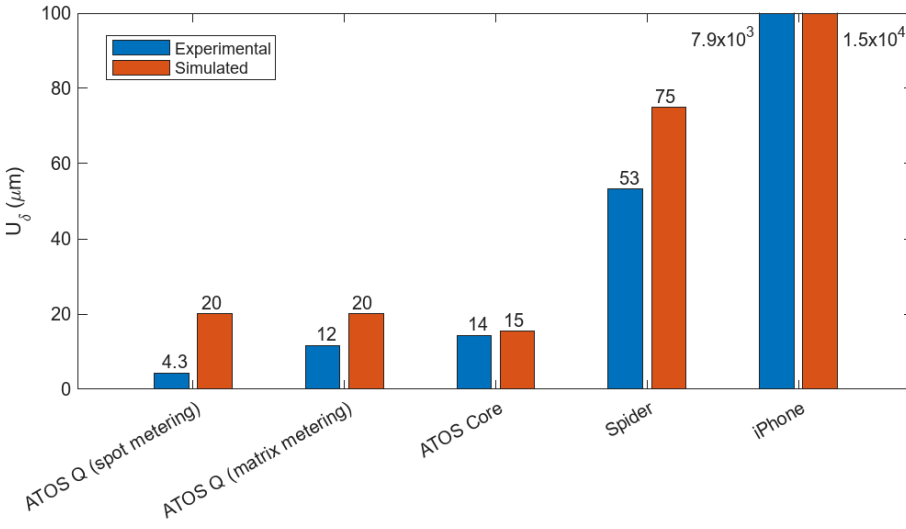


FIGURE 8. Expanded uncertainty of translation (top) and rotation (bottom) for experimental and Monte Carlo simulation approaches.

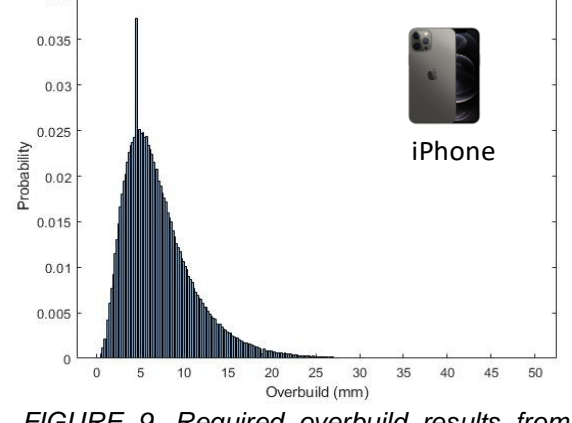
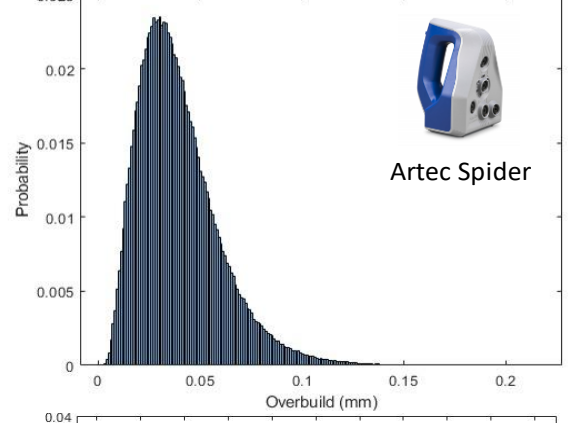
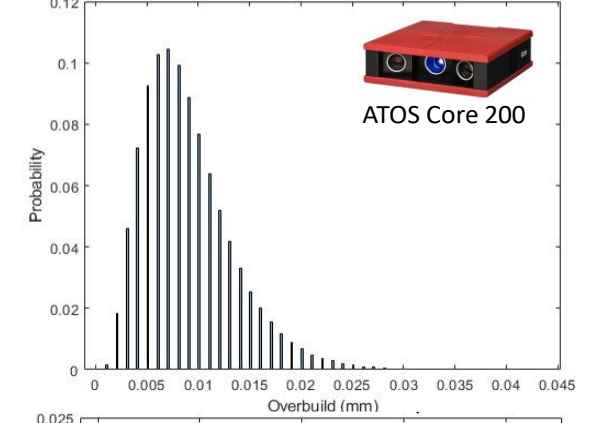
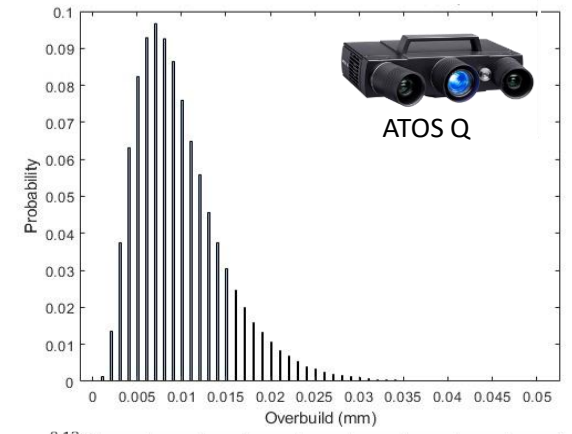


FIGURE 9. Required overbuild results from Monte Carlo simulation.